Photopatternable Di-ureasil−Zirconium Oxocluster Organic−Inorganic Hybrids As Cost Effective Integrated Optical Substrates

Daniela C. Oliveira,[†] Andreia G. Macedo,[‡] Nuno J. O. Silva,[§,‡] Celso Molina, Rute A. S. Ferreira,[‡] Paulo S. André,[||] Karim Dahmouche,[⊥] Verónica De Zea Bermudez,[#] Younes Messaddeq,[†] Sidney J. L. Ribeiro,*[,†] and Luís D. Carlos*[,‡]

Institute of Chemistry, São Paulo State University, UNESP, C.P. 355, 14801-970, Araraquara-SP, Brazil, Department of Physics, CICECO, and Instituto de Telecomunicações, University of Aveiro, 3810−193 Aveiro, Portugal, Universidade Estadual da Zona Oeste (UEZO), Campo Grande 23070-200, Rio de Janeiro-RJ, Brazil, and Departamento de Química and CQ-VR, Universidade de Trás-os-Montes e Alto Douro, 5000-801 Vila Real, Portugal

Received November 6, 2007. Revised Manuscript Received February 27, 2008

Organic−inorganic hybrids containing methacrylic acid (McOH, CH_2=$C(CH_3)COOH$)) modified zirconium tetrapropoxide, $Zr(OPr^n)_4$, classed as di-ureasil−zirconium oxo-cluster hybrids, have been prepared and structurally characterized by X-ray diffraction (XRD), small-angle X-ray scattering (SAXS), Fourier transform infrared (FT-IR) and Raman (FT-Raman) spectroscopies, ^{29}Si and ^{13}C nuclear magnetic resonance (NMR), and atomic force microscopy (AFM). XRD and SAXS results have pointed out the presence of Si- and Zr-based nanobuilding blocks (NBBs) dispersed into the organic phase. Inter-NBBs correlation distances have been estimated for the pure di-ureasil and a model compound obtained by hydrolysis/condensation of $Zr(OPr^n)_4$:McOH (molar ratio 1:1): $d_{Si} \approx 26 \pm 1$ Å and $d_{Zr} \approx 16 \pm 1$ Å, respectively. In the case of the di-ureasil−zirconium oxo-cluster hybrids, these distances depend on the Zr relative molar percentage (rel. mol. Zr %) (d_{Si} ranges from 18 to 25 Å and d_{Zr} from 14 to 23 Å, as the rel. mol. Zr % increases from 5 to 75), suggesting that the Si- and Zr-based clusters are interconstrained. Complementary data from FT-IR, FT-Raman, ^{29}Si and ^{13}C NMR, and AFM support to a structural model where McOH-modified Zr-based NBBs (Zr-OMc) are present over the whole range of composition. At low Zr-OMc contents (rel. mol. Zr % <30) the clusters are well-dispersed within the di-ureasil host, whereas segregation occurs at the 0.1 μm scale at high Zr-OMc concentration (rel. mol. Zr % = 50). No Zr−O−Si heterocondensation has been discerned. Monomode waveguides, diffractions gratings, and Fabry−Perot cavities have been written through the exposure of the hybrid monoliths to UV light. FT-Raman has shown that the chemical process that takes place under illumination is the polymerization of the methacrylate groups of the Zr-OMc NBBs. The guidance region in patterned channels is a Gaussian section located below the exposed surface with typical dimensions of 320 μm wide and 88 μm deep. The effective refractive index is 1.5162 (maximum index contrast on the order of 1×10^{-4}) and the reflection coeficient of the Fabry−Perot cavity (formed by a grating patterned into a 0.278 cm channel) is 0.042 with a free spectral range value of 35.6 GHz.

1. Introduction

The potential applications of the so-called organic−inorganic hybrids in many different areas, including integrated optics (IO), has been extensively explored during the last years.[1–3] The simplicity and low cost of the sol−gel process make this method very suitable for the development of organic−inorganic hybrid materials for the production of functional IO devices.[4,5] Among the huge quantity of available precursors, the combination of organic−inorganic hybrids with methacrylic acid (McOH) modified metal oxide precursors (namely zirconium tetrapropoxide, $Zr(OPr^n)_4$) has been recursively used for the fabrication of low cost IO devices.[6–8] Concerning optical properties, the main role of $Zr(OPr^n)_4$ in organic−inorganic

* Corresponding author. Tel.: 351-234370946(L.D.C.); 55-16-33016631 (S.J.L.R.). Fax: 351-234378197 (L.D.C.); 55-16-33016692 (S.J.L.R.). E-mail: lcarlos@ua.pt (L.D.C.); sidney@iq.unesp.br (S.J.L.R.).

[†] São Paulo State University.

[‡] Department of Physics, CICECO, University of Aveiro.

[§] Present address: Instituto de Ciencia de Materiales de Aragón CSIC/ Universidad de Zaragoza, Spain.

[||] Department of Physics and Instituto de Telecomunicações, University of Aveiro.

[⊥] Universidade Estadual da Zona Oeste.

[#] Universidade de Trás-os-Montes e Alto Douro.

(1) Sanchez, C.; Julian, B.; Belleville, P.; Popall, M. *J. Mater. Chem.* **2005**, *15*, 3559.

(2) Sanchez, C.; Lebeau, B.; Chaput, F.; Boilot, J.-P. *Adv. Mater.* **2003**, *15*, 1969.

(3) Houbertz, R.; Domann, G.; Cronauer, C.; Schmitt, A.; Martin, H.; Park, J. U.; Frohlich, L.; Buestrich, R.; Popall, M.; Streppel, U.; Dannberg, P.; Wachter, C.; Brauer, A. *Thin Solid Films* **2003**, *442*, 194.

(4) *Functional Hybrid Materials*; Gomez-Romero, P., Sanchez, C., Eds.; Wiley Interscience: New York, 2003.

(5) Carlos, L. D.; Sá Ferreira, R. A.; de Zea Bermudez, V. Hybrid Materials for Optical Applications. In *Hybrid Materials: Synthesis, Characterization, and Applications*; Kickelbick, G., Ed.; Wiley Interscience: New York, 2007; Vol. 337.

(6) Schmidt, H.; Krug, H.; Kasemann, R.; Tiefensee, F. In *Submolecular Glass Chemistry and Physics*; Bray, P., Kreidl, N. J., Eds.; Proceedings SPIE 1590; International Society for Optical Engineering: Bellingham, WA, 1991; p 36.

10.1021/cm7031702 CCC: $40.75
Published on Web 05/10/2008

hybrids is to achieve a fine control over the refractive index. In the presence of McOH, a fraction of the propoxy groups of $Zr(OPr^n)_4$ is substituted by carboxylate moieties and a new molecular precursor, with a different structure and lower reactivity, results. Different crystalline phases have been characterized in systems composed of zirconium alkoxides and McOH. Methacrylate-capped metal-oxo clusters have been identified in these crystalline phases[9] and by varying the Zr:McOH ratio, clusters with a different size and shape and a different degree of substitution can be obtained.[9–13] For instance, when $Zr(OPr^n)_4$ is reacted with an excess of McOH (molar ratio $Zr(OPr^n)_4$:McOH 1:2), the $Zr_6(OH)_4O_4(OMc)_{12}$ cluster is formed in which chelating and bridging OMc^- ligands cover the surface. The structure of the cluster core is analogous to the basic structural unit of tetragonal zirconia[9] and those functional NBBs have been used in the preparation of new polymers where structurally well-defined oxo-metalate clusters are covalently incorporated.[13–17]

Among the various organic−inorganic hosts that have been developed in the last years, the so-called di-ureasils[5,18–21] present acceptable transparency, mechanical flexibility, and thermal stability to be processed as thin films and be used as the organically modified silicate host together with lanthanide ions,[22] Coumarine-153 laser dye,[23] Ti species,[24] and McOH-modified $Zr(OPr^n)_4$.[25,26] In the latter case, distributed feedback lasers were demonstrated using dynamic gratings and rodhamine 6G doping.[27] Furthermore, gratings, channel, and monomode planar waveguides with low propagation losses, both in the infrared (0.6−1.1 dB/cm) and in the visible (0.4−1.5 dB/cm), were fabricated using the synergism between two hybrid precursors (di-ureasil and methacryloxypropyltrimethoxysilane) and McOH-modified $Zr(OPr^n)_4$.[26]

The technological perspectives for the IO devices indicate that one of the possible utilization is on the implementation of low cost passive all-optical networks operating at high bit rate optical signals (40 Gbits/s), bringing then the optical to the home. This will require low-cost components to operate in the infrared spectral region, typically at 1550 nm. Examples of applications are narrow band optical filters, low-loss optical power splitters, and optical cavities (for the optical clock extraction function). A window of opportunity for sol−gel derived components is therefore opened.

Di-ureasil−zirconium oxo-cluster hybrids are promising candidates for low cost components of IO devices since (i) they can be processed either as transparent monoliths (tailored with the desired shape) or thin, transparent, and uniform films;[25–27] (ii) the control over the refractive index is easily achieved through $Zr(OPr^n)_4$ addition,[26] (iii) they can incorporate different light-emitting centers (lanthanide ions and organic dyes),[22,23,27] and (iv) the hybrid host displays photosensitivity allowing patterning. Moreover, di-ureasil−zirconium oxo-cluster hybrids meet the thermal standards used to qualify the reliability of IO components, maximum thermal stability up to +70 °C.[28] Although di-ureasils tend to present a yellowish hue,[29] it will not impact the optical functionalities addressed here because they occurred in the infrared spectral range (1550 nm).

With these properties in mind, the initial purpose of this work was to characterize in detail the structural features of di-ureasil−zirconium oxo-cluster hybrids using small-angle X-ray scattering (SAXS), X-ray diffraction (XRD), atomic force microscopy (AFM), nuclear magnetic resonance (NMR), and Fourier transform infrared (FT-IR) and Raman (FT-Raman) spectroscopies. Another aim was to write monomode waveguides through the exposure of the hybrid monoliths to UV light. To illustrate the feasibility of the di-ureasils as cost-effective IO substrates, we superimposed UV patterned diffraction gratings in these waveguides, forming Fabry−Perot cavities. The chemical process behind photopatterning and the waveguide region were studied, permitting the determination of its effective refractive index and the maximum index contrast.

2. Experimental Section

Nonhydrolyzed Di-ureasil Precursor (d-UPTES(600)). The organic−inorganic hybrid framework d-U(600) is composed of polyether-based chains grafted at both ends to a siloxane backbone

(7) Najafi, S. I.; Touam, T.; Sara, R.; Andrews, M. P.; Fardad, M. A. J. *Lightwave Technol.* **1998**, *16*, 1640.
(8) Etienne, P.; Coudray, P.; Porque, J.; Moreau, Y. *Opt. Commun.* **2000**, *174*, 413.
(9) Schubert, U. *Chem. Mater.* **2001**, *13*, 3487.
(10) Schubert, U.; Arpac, E.; Glaubitt, W.; Helmerich, A.; Chau, C. *Chem. Mater.* **1992**, *4*, 291.
(11) Kickelbick, G.; Schubert, U. *Chem. Ber.* **1997**, *130*, 473.
(12) Kickelbick, G.; Wiede, P.; Schubert, U. *Inorg. Chim. Acta* **1999**, *284*, 1.
(13) Kogler, F. R.; Jupa, M.; Puchberger, M.; Schubert, U. J. *Mater. Chem.* **2004**, *14*, 3133.
(14) Trimmel, G.; Fratzl, P.; Schubert, U. *Chem. Mater.* **2000**, *12*, 602.
(15) Trimmel, G.; Gross, S.; Kickelbick, G.; Schubert, U. *Appl. Organomet. Chem.* **2001**, *15*, 401.
(16) Schubert, U.; Völkel, T.; Moszner, N. *Chem. Mater.* **2001**, *13*, 3811.
(17) Faccini, F.; Eric, H.; Schubert, U.; Wendel, E.; Tsetsgee, O.; Muller, K.; Bertagnolli, H.; Venzo, A.; Gross, S. *J. Mater. Chem.* **2007**, *17*, 3297.
(18) de Zea Bermudez, V.; Carlos, L. D.; Alcácer, L. *Chem. Mater.* **1999**, *11*, 569.
(19) Carlos, L. D.; de Zea Bermudez, V.; Sá Ferreira, R. A.; Marques, L.; Assunção, M. *Chem. Mater.* **1999**, *11*, 581.
(20) Carlos, L. D.; Sá Ferreira, R. A.; de Zea Bermudez, V.; Ribeiro, S. J. L. *Adv. Funct. Mater.* **2001**, *2*, 111.
(21) Carlos, L. D.; Sá Ferreira, R. A.; Pereira, R. N.; Assunção, M.; de Zea Bermudez, V. *J. Phys. Chem. B* **2004**, *108*, 14924.
(22) Carlos, L. D.; Messaddeq, Y.; Brito, H. F.; Sá Ferreira, R. A.; de Zea Bermudez, V.; Ribeiro, S. J. L. *Adv. Mater.* **2000**, *12*, 594.
(23) Stathatos, E.; Lianos, P.; Lavrencic Stangar, U.; Orel, B. *Chem. Phys. Lett.* **2001**, *345*, 381.
(24) Molina, C.; Dahmouche, K.; Hammer, P.; de Zea Bermudez, V.; Carlos, L. D.; Ferrari, M.; Montagna, M.; Gonçalves, R. R.; Oliveira, L. F. C.; Edwards, H. G. M.; Messaddeq., Y.; Ribeiro, S. J. L. *J. Braz. Chem. Soc.* **2006**, *17*, 443.
(25) Sá Ferreira, R. A.; Molina, C.; Dahmouche, K.; Ribeiro, S. J. L.; Gonçalves, R. R.; de Zea Bermudez, V.; Carlos, L. D. *Mater. Res. Soc. Symp. Proc.* **2004**, *847*, 63.
(26) Molina, C.; Moreira, P. J.; Gonçalves, R. R.; Sá Ferreira, R. A.; Messaddeq, Y.; Ribeiro, S. J. L.; Soppera, O.; Leite, A. P.; Marques, P. V. S.; de Zea Bermudez, V.; Carlos, L. D. J. *Mater. Chem.* **2005**, *15*, 3937.
(27) Oliveira, D. C.; Messaddeq, Y.; Dahmouche, K.; Ribeiro, S. J. L.; Gonçalves, R. R.; Vesperini, A.; Gindre, D.; Nunzi, J.-M. *J. Sol−Gel Sci. Technol.* **2006**, *40*, 359.
(28) *Generic Reliability Assurance Requirements for Passive Optical Components*; GR-1221-CORE; Bellcore/Telcordia: New York, January 1999; issue 2.
(29) Boev, V. I.; Soloviev, A.; Silva, C. J. R.; Gomes, M. J. M.; Barber, D. J. *J. Sol−Gel Sci. Technol.* **2007**, *41*, 223.

Scheme 1. Schematic Representation of the Synthesis of the ZPO-OMc Material

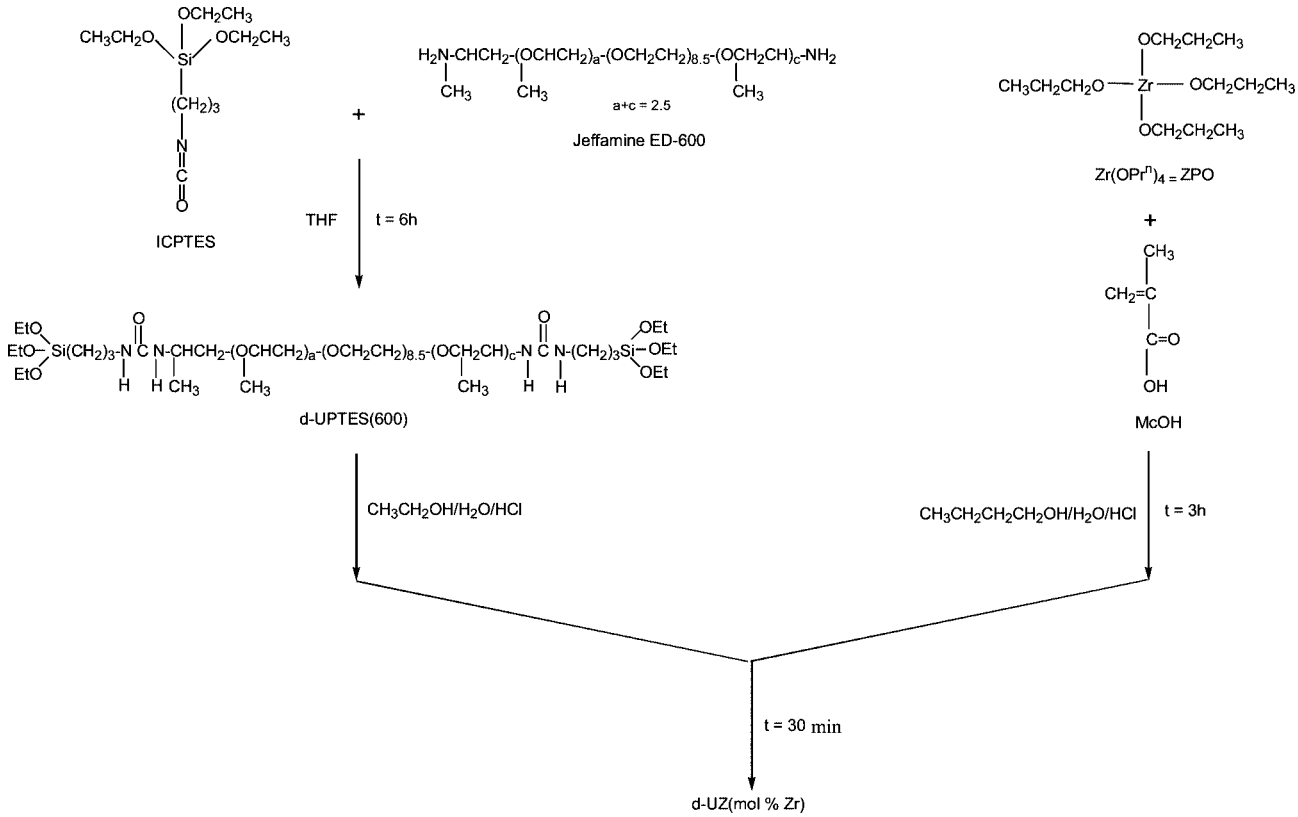

through urea functionalities.[18–20] The urea linkages were formed between the terminal amine groups of a double functional diamine (O,O′-Bis-(2-aminopropyl) polypropylene glycol-block-polyethylene glycol-block-polypropylene glycol, commercially designated as Jeffamine ED-600, Fluka, average molecular weight MW $\approx$ 600 g mol^{-1}) and the isocyanate group of an alkoxysilane precursor (3-isocyanatopropyltriethoxysilane, ICPTES, Fluka), molar ratio ICPTES:Jeffamine ED-600=2:1. The resulting mixture was stirred at room temperature for 6 h in tetrahydrofuran (THF, Merck) to yield the diureapropyltriethoxysilane (d-UPTES(600))[18] precursor (Scheme 1A).

McOH-Modified Zr(OPr^n)$_4$. The precursor used in the preparation of the hybrid materials, named hereafter as Zr-OMc, together with d-UPTES(600), was obtained by mixing Zr(OPr^n)$_4$ (Fluka) and McOH (CH_2=C(CH_3)C(=O)OH, Fluka) at room temperature with a 1:1 Zr(OPr^n)$_4$:McOH molar ratio in butanol ($CH_3(CH_2)_3OH$, BuOH, Fluka) and stirred for 3 h (Scheme 1B).

Model Compounds. In addition to the latter precursor solution, three powdered compounds were synthesized by mixing Zr(OPr^n)$_4$, McOH and ethanol (CH_3CH_2OH, EtOH, Fluka) in different Zr(OPr^n)$_4$:McOH:EtOH molar ratios (10:1:3, 1:1:3, and 1:10:3). From the resulting transparent solutions, wet gels were obtained and dried at room temperature in open flasks, resulting in white powders named hereafter as Z10:1, Z1:1, and Z1:10, respectively. A McOH free compound (designated as ZPO) was also prepared just by hydrolysis and condensation of Zr(OPr^n)$_4$. Because of its high reactivity, Zr(OPr^n)$_4$ can absorb water from the air (typically about 50% moisture) and consequently readily hydrolyze and condensate quickly, forming a white powder.

Di-ureasil−ZPO-OMc hybrids. The Zr-OMc and d-UPTES(600) precursors were prehydrolyzed with a hydrochloric acid solution (HCl 0.01 mol L^{-1}), with a water-to-metal (Zr and Si) molar ratio of 0.5:4 (parts A and B in Scheme 1). The prehydrolyzed solutions were mixed with Zr relative molar percentage (rel. mol. Zr %) from 5 to 75. Deionised water was added (H_2O:(Si + Zr) = 3) and the final sol obtained was stirred for 30 min. It is noteworthy that the maximum Zr concentration depends on the nature of the alcohol used in the preparation of the Zr-OMc precursor. In EtOH, for instance, only a rel. mol. Zr % of 30−35 could be incorporated without precipitation. The transparent sols were poured into molds and placed at ambient conditions until gelation occurred. The wet gels were further dried at around 50 °C until transparent xerogels were obtained. The di-ureasil−ZPO-OMc hybrids will be henceforth identified as d-UZ(X rel. mol. Zr %), with X = 9, 15, 17, 23, 33, 40, 47, 50, 60, 75.

Fabrication of Monomode Waveguides and Gratings. The waveguide writing was performed in the monoliths through the exposure to a c.w. Ar-ion laser frequency doubled (244 nm) by a BBO (BaB_2O_4) crystal operating at 40 mW. The laser beam was shaped by an iris in order to remove spatial noise and by a plano-cylindrical lens to create a narrow laser line with 2 mm length. The laser line was then translated by a motorized positioning system in order to create the waveguide region. The speed of the translation was varied between 0.02 and 0.06 mm/s. Diffraction gratings were recorded using a modified Talbot interferometer. One phase mask was used to split the incident beam in the $\pm$1 orders signals. The 0 order, which was also generated, was blocked just after the phase mask. The $\pm$1 order signals were reflected by two external mirrors, and interfered in a designate focal point, where the sample was placed. The main advantage of this method resides in the easier alteration of the focal point and therefore of the interference conditions that result in a change of the interference period, giving extra tunability. A diffraction grating was written in the middle of a short length waveguide (0.278 cm) previously patterned in order to produce a Fabry−Perot cavity. The monolith/air interface acts as reflectors of the cavity with a reflection coefficient (R) given by the Fresnell law for perpendicular interference

$$R = \left(\frac{n_{\text{eff}} - n_{\text{air}}}{n_{\text{eff}} + n_{\text{air}}}\right)^2 \quad (1)$$

where n_{eff} and n_{air} are the refractive index of the monolith in the waveguide region and that of the air, respectively.

Small-Angle X-ray Scattering (SAXS). Measurements were performed in National Synchrotron Light Laboratory (LNLS), Campinas, Brazil, using its SAXS beam line which provides a monochromatic ($\lambda = 1.608$ Å) and horizontally focused beam. The intensity was recorded as a function of the modulus of the scattering vector q (where $q = (4\pi/\lambda)\sin(\epsilon/2)$, ϵ being the scattering angle). Because of the small size of the incident beam cross section at the detection plane, no mathematical desmearing of the experimental SAXS intensity was needed. Each spectrum corresponds to a data collection period of 300 s. The relative error of the SAXS intensity evaluated from the statistical variance associated with the number N_f of photons collected during data acquisition is

$$\frac{\Delta I(q)}{I(q)} = \frac{2}{\sqrt{N_f}}$$

The relative error was significant only over the high q scattering intensities. The parasitic scattering intensity from air, slits, and windows was subtracted from the total intensity. The scattering intensity was also normalized by taking into account the varying intensity of the direct X-ray beam, sample absorption, and sample thickness.

Powder X-ray Diffraction (XRD). XRD patterns were recorded using a Philips X'Pert MPD powder X-ray diffractometer. The samples were exposed to the Cu Kα radiation (1.54 Å) in a 2θ range between 1 and 70°, with a resolution of 0.05° and an acquisition time of 35 s per point.

Atomic Force Microscopy (AFM). The images were obtained using a AFM Nanoscope Instruments equipment, in tapping mode, with a super sharp silicon probe having a radius of 10 nm, resonance frequency 330 kHz and spring constant 42 N/m. The images were deconvoluted considering the probe's shape using the WSXM software.[30] To improve the image quality, we used tools to flatten and eliminate line noise and a Gaussian filter. The same tip was employed in all the images recorded to avoid the influence of the tip radius variations on the square roughness values.

Fourier Transform Infrared Spectroscopy (FT-IR). Midinfrared spectra were acquired at room temperature using a Unicam FT-IR system. The spectra were collected over the range 4000−400 cm^{-1} by averaging 60 scans at a maximum resolution of 4 cm^{-1}. Solid samples (2 mg) were finely ground and analyze by dispersing them in approximately 175 mg of dried spectroscopic grade potassium bromide (KBr, Merck) by the pressed-disk technique. The disks were vaccuum-dried at 90 °C for a long period of time in order to reduce the levels of solvent and adsorbed water in the samples prior to recording the spectra under ambient conditions. Consecutive spectra were recorded until reproducible results were obtained. The evaporation was infrared-monitored in the OH region.

FT-Raman Scattering. The FT-Raman spectra were recorded using a Bruker RFS 100/S spectrometer, operating with a Nd:YAG laser excitation (1064 nm at 400 mW) by averaging 200 scans at a maximum resolution of 4 cm^{-1}.

Nuclear Magnetic Resonance (NMR). ^{29}Si magic-angle spinning (MAS) and ^{13}C cross-polarization (CP) MAS NMR spectra were recorded using a Bruker Avance 400 (9.4 T) spectrometer (DSX model) at 79.49 and 100.62 MHz, respectively. A rf pulse length of 2 μs (equivalent to 30° flip angle), a recycle delay of 60 s, and a spinning rate of 5.0 kHz were employed to record the ^{29}Si MAS NMR spectra, whereas for the ^{13}C CP/MAS spectra the values were 2.8 μs (equivalent to 45° flip angle), 4 s, and 8 kHz, respectively. Chemical shifts are quoted in ppm from tetramethylsilane (TMS).

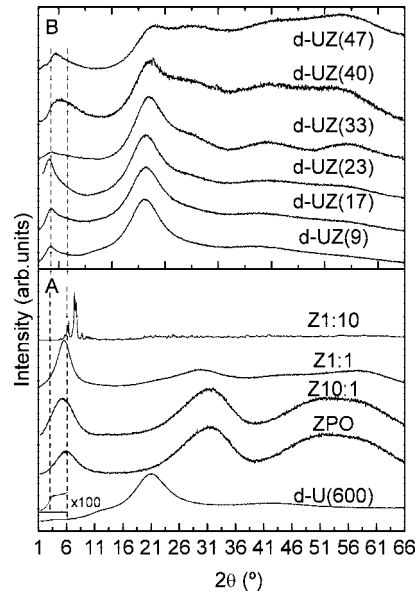

Figure 1. XRD patterns of (A) d-U(600) and powdered ZPO, Z10:1, Z1:1, and Z1:10 model compounds; (B) d-UZ(9), d-UZ(17), d-UZ(23), d-UZ(33), d-UZ(40), and d-UZ(47) hybrids.

Mode Field Distribution. The mode field distribution was acquired using a xyz positioning system and a laser beam profiler from Newport LPB-1 with microscope objective. The measurements were made with two lasers operating at 632 and 980 nm. The signals were coupled into the waveguide region patterned previously, using an optical fiber and the positioning system to excite a propagation mode. The output mode profile was measured with a beam profile analyzer with an integration time of 10 s and *xy* position experimental error of 0.15 μm.

Reflection Spectrum. The reflection grating spectrum of the monolithic sample was obtained with an Amonics ALS-CL-17optical broadband source covering the spectral region between 1530 and 1620 nm. The signal was coupled to the waveguide using a standard monomode optical fiber. In order to minimize the optical losses in the coupling, an index matching gel (Thorlabs) was used. An optical circulator monitored the reflected spectrum, measured with an optical spectrum analyzer (Advantest Q8384).

3. Results and Discussion

3.1. Structural Features. Figure 1A shows the XRD patterns of d-U(600) and of the ZPO, Z10:1, Z1:1, and Z1:10 model compounds. With the exception of the Z1:10 pattern, the remaining ones display broad peaks characteristic of amorphous materials. The broad hump centered at $2\theta = 21.5°$, clearly discerned for d-U(600), is associated with the presence of amorphous siliceous domains,[19] corresponding to an intradomain characteristic structural mean distance of $r = 4.2$ Å. The second order of this structural unit appears at $2\theta \approx 45°$. The structural unit distance r obtained is equal to that reported for vitreous SiO_2, being larger than the Si−O, O−O, and Si−Si distances, (1.62, 2.65, and 3.12 Å, respectively), and represents the building-up of correlations whose basic period is well beyond the first few near-neighbor

(30) Horcas, I.; Fernandez, R.; Gómez-Rodrigues, J. M.; Colchero, J.; Gómez-Herrero, J.; Baro., A. M. *Rev. Sci. Instrum.* **2007**, *78*, 013705.

distances. In the low-angle region of the d-U(600) XRD pattern a peak is observed at $2\theta = 3.4°$ (amplified region of the d-U(600) pattern of Figure 1A). This peak was assigned to a spatial correlation between the siliceous domains embedded in a polymer-rich medium.[19,31] This assignment was made on the basis of the fact that the peak position shifts to lower angles with the increase of the polymer molecular weight.[31] The intersiliceous domains distance (d_{Si}) of d-U(600) is ~26 Å.

The diffraction pattern exhibited by the ZPO sample displays broad peaks centered around $2\theta = 30$, 50, and 60° that correspond to the main features of tetragonal zirconia (ZrO_2).[32] This basic tetragonal molecular unit is in fact also observed in the core of the Zr-OMc NNBs.[9] In the low-angle region of the same diffractogram, the peak distinctly observed at $2\theta \approx 6.0°$ is associated to an inter-Zr clusters characteristic distance (d_{Zr}) of ~14 Å. The diffraction pattern obtained for the sample Z10:1 displays essentially the same features observed for the ZPO sample, with an increase in the relative intensity of the low angle peak being observed. As the OMc-content increases, this peak becomes narrower and shifts to lower angles being situated at $2\theta = 5.5°$ for the Z1:1 sample, an indication of an increase in the size and/or order of the clusters. In the case of the Z1:10 sample, several narrow peaks become apparent in the low-angle region showing the existence of "long-range-ordered clusters", i.e., crystals. In fact, the formation of clusters that arrange themselves into large ordered structures after the hydrolysis and condensation of Zr alkoxides has been reported, including the case of the hydrolysis of $Zr(OPr^n)_4$ in the presence of McOH.[10–13] These McOH-modified Zr NBBs are arranged along different crystal structures, with unit-cell dimensions on the order of the characteristic intercluster distance found for the d-UZ samples (d_{Zr} = 15−23 Å, as demonstrated bellow), and with the cluster type/arrangement depending on the $Zr(OPr^n)_4$:McOH ratio.[13,10–12] The d_{Zr} value estimated from the peak observed at the low-angle region of the diffraction patterns presented in Figure 1A must therefore correspond to a characteristic distance due to a less-ordered (amorphous) arrangement of similar Zr-OMc NBBs.

The same broad peaks observed for the d-U(600) and ZPO model compounds are identified in the d-UZ hybrids (Figure 1B). The wide angle region of their XRD patterns display two convoluted peaks, associated with order within the siliceous domains and Zr cluster core. As the position of these peaks is neither changed along the d-UZ series, nor resembles that of the peaks of the d-U(600) and ZPO materials alone, we are led to conclude that Zr−Si heterocondensation reactions are unlikely.

The two peaks seen in the low-angle region ($2\theta < 7°$) of the d-UZ XRD patterns, correspond to those observed in the XRD patterns of d-U(600) and ZPO, associated with the d_{Zr} and d_{Si} distances (dashed lines in Figure 1B), corroborating the idea that the individual structural units have been preserved. This low angle region is better analyzed in the

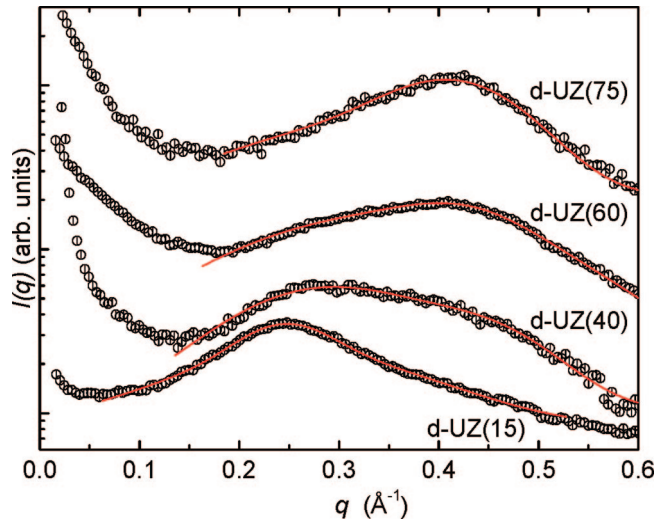

Figure 2. SAXS curves of the d-UZ(15), d-UZ(40), d-UZ(60), and d-UZ(75) hybrids (open circles) and fits to eq 2 (solid lines).

SAXS curves shown in Figure 2. For $q > 0.1$ Å^{-1}, the scattered intensity is dominated by the two peaks observed in the low-angle region of the XRD patterns. The total intensity I is taken as the product of a form factor $P(q)$ and a structure factor $S(q)$.[33] As in the $0.1 < q < 0.6$ Å^{-1} region I is dominated by $S(q)$, $P(q)$ can be considered constant. $S(q)$ is the sum of two Gaussian curves

$$S(q) = \frac{A_1}{q\sigma_{Si}\sqrt{2\pi}} \exp\left[-\frac{(q-q_{Si})^2}{2\sigma_{Si}^2}\right] + \frac{A_2}{q\sigma_{Zr}\sqrt{2\pi}} \exp\left[-\frac{(q-q_{Zr})^2}{2\sigma_{Zr}^2}\right] \quad (2)$$

where A_1 and A_2 are the areas of the peaks associated to the intersiliceous domains and inter-Zr cluster order, respectively, and σ_{Si} and σ_{Zr} are the corresponding full-width at half-maximum (fwhm). The relation between d_{Si} and d_{Zr} with q_{Si} and q_{Zr}, respectively, is given by $d_{Si} = 2\pi/q_{Si}$ and $d_{Zr} = 2\pi/q_{Zr}$. Figure 3 shows the d_{Si} and d_{Zr} correlation distances as a function of the Zr-OMc content in d-UZ hybrids. At low Zr-OMc content, whereas d_{Si} is close to the characteristic value of the d-U(600) host,[31,34] d_{Zr} is higher than the value found for Z1:1 model compound (1:1) (Table 1 and Figure 3) Upon increasing the Zr-OMc content, these two distances decrease, with d_{Zr} approximating the value found for Z1:1 (15.9 Å) (Figure 3). This behavior can be explained by a structural model where for low Zr-OMc content the Zr-based molecular clusters are embedded in the polymeric phase between the siliceous domains leading to the observation of higher d_{Zr} correlation distance. For high Zr-OMc content, segregation of the individual components occurs and thus d_{Zr} approaches the value characteristic of Z1:1 model compound. This indicates that the Si- and Zr-based networks are interconstrained.

At the low q region of the SAXS patterns of the d-UZ hybrids ($q < 0.1$ Å^{-1}), it is possible to observe the onset of a power law associated with an increase of the electron

(31) Dahmouche, K.; Santilli, C. V.; Pulcinelli, S. H.; Craievich, A. F. J. *Phys. Chem. B* **1999**, *103*, 4937.
(32) Teufer, G. *Acta Crystallogr.* **1962**, *15*, 1187.
(33) See, for instance: Porod, G. In *Small Angle X-ray Scattering*; Glatter, O., Kratky, O., Eds.; Academic Press: New York, 1982.
(34) Dahmouche, K.; Carlos, L. D.; de Zea Bermudez, V.; Sá Ferreira, R. A.; Santilli, C. V.; Craievich, A. F. J. *Mater. Chem.* **2001**, *11*, 3249.

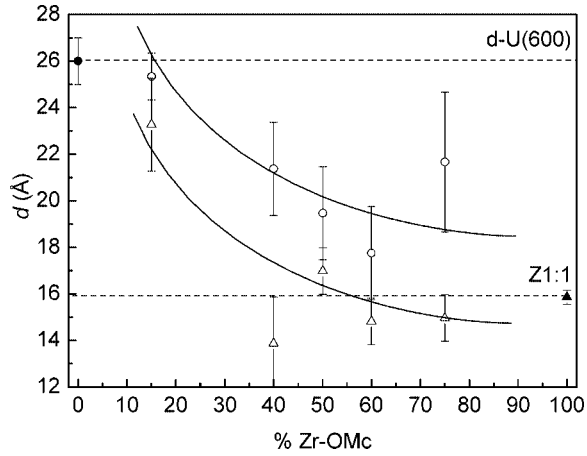

Figure 3. Correlation distances, d_{Si} (open circles) and d_{Zr} (open triangles), as a function of the Zr-OMc content in the d-UZ hybrids obtained from SAXS data. The structural distances of the d-U(600) and Z1:1 compounds are represented as a filled circle and a filled triangle, respectively. The lines are guide for the eyes.

density and/or size of the scattering entities. It is expected that this power law is followed by an exponential law, at angles lower than those studied here, from which the characteristic size of these scattering entities would be estimated. Because no exponential law is visible down to the lowest measured q (0.015 Å^{-1}), the characteristic size of these scattering entities should be larger than 70 nm. These larger entities, associated to secondary Zr-rich aggregates as reported for zirconia-silica dye-doped films,[35] are clearly identified in AFM images (Figure S1 of the Supporting Information). The size distribution of these aggregates was calculated giving average values ranging from 300 to 500 nm (standard deviation between 20 and 35%) as the Zr-OMc content (rel. mol. Zr %) increases from 17 to 40%.

The ^{29}Si MAS NMR spectrum of d-UZ(23) is depicted in Figure 4A together with that obtained for the d-U(600) sample.[36] The d-UZ(23) spectrum exhibits three wide peaks at approximately −50, −58, and −60 ppm, ascribed to organosiloxane entities R′Si(OSi)-(OR)$_2$ (T_1), R′Si(OSi)$_2$(OR) (T_2), and R′Si(OSi)$_3$ (T_3), respectively.[36,37] Upon varying the Zr-OMc concentration, no significant changes result in the ^{29}Si MAS NMR spectra (not shown), indicating that even at higher concentrations there is no effective interaction between the Zr-based clusters and the siliceous nanodomains. Comparison of these spectra with that of d-U(600)[36] allows to infer that the presence of Zr-OMc clusters leads to an increase in the population of T_2 sites and the appearance of T_1 sites. Therefore the occurrence of Zr-OMc clusters constrains the siliceous network formation, leading to less branched arrangements for the siliceous backbone domains with respect to d-U(600). The degree of condensation, c, has been calculated according to the expression $c = 1/3(\%T_1 + 2\%T_2 + 3\%T_3)$[37] As previously reported,[25] the d-UZ hybrids have condensation degree values in the 86−90% range, thus lower than that of d-U(600) (96%).[36]

Figure 4B shows the ^{13}C CP/MAS NMR spectra for d-U(600) and d-UZ(23). For other Zr-OMc concentrations (spectra not shown) no significant differences are discerned, similarly to the situation found for the ^{29}Si MAS NMR spectra. The two spectra of Figure 4B are very similar, except for the presence of two additional low-intensity peaks at 14.9 ppm and 125.6 ppm in the case of d-UZ(23). These resonances are ascribed to $=CH_3$ and $=CH_2$ carbons in McOH.[38] The similarity between the ^{13}C CP/MAS NMR spectra of the d-UZ hybrids and that of d-U(600) suggests that the Zr-OMc aggregates do not interact with the polyether chains. Therefore, NMR data are in accord with the structural model depicted previously (based on XRD and SAXS results) reinforcing the interconstraining between the Zr- and Si-based phases mentioned above.

Figure 5 displays FT-IR spectra obtained by subtracting the spectrum of d-U(600) from those of the d-UZ hybrids. This procedure allowed us to discriminate the spectral changes to which the most characteristic bands of ZPO and McOH that appear between 2000 and 500 cm^{-1} are subject after adding these compounds to d-U(600), since this hybrid host absorbs strongly in this interval.[18] No characteristic contribution of the stretching vibration of the C═O groups (υC═O) of the monomeric ("free") form of McOH, expected at about 1750 cm^{-1},[39] is observed. The feature characteristic of the presence of hydrogen-bonded ether-McOH aggregates,[39] typically seen at 1728 cm^{-1}, is also absent. The weak ill-defined band detected around 1707 cm^{-1} (Figure 5) is tentatively assigned to the υC═O of the dimeric (self-associated) form of McOH,[17,39]

Because all the methacrylate groups appear to be coordinated, it is of interest to inspect the 1640−1320 cm^{-1} band envelope of the d-UZ hybrids, where the antisymmetric and symmetric stretching vibration modes of the COO$^-$ group (υ_{as}COO and υ_sCOO, respectively) are expected. Prior to discussing in detail this spectral region, we emphasize that carboxylate groups can coordinate to a metal in three possible ways (Figure S2 of the Supporting Information). The wavenumber separation $\Delta\bar{\upsilon}$ between the υ_{as}COO and υCOO modes in a bridging configuration usually lies between 120 and 160 cm^{-1}. Lower values are indicative of chelate bonding.[40]

Features at 1589, 1552, 1529, 1460, 1423, and 1373 cm^{-1} are distinctly seen in the subtraction spectra of the d-UZ diureasils reproduced in Figure 5. The pair of bands at 1552 and 1423 cm^{-1}, also detected in the infrared spectrum of the Z1:1 compound, may be assigned to the υ_{as}COO$^-$ and υ_sCOO$^-$ modes, respectively.[10] This finding strongly suggests the presence of bidentate bridging configuration ($\Delta\bar{\upsilon} \approx 130$ cm^{-1}) in all the materials. On the basis of FT-IR data of a recent report focused on Zr oxoclusters,[38] we tentatively attribute the remaining bands of this region at 1589 and 1529 cm^{-1} to the υ_{as}COO mode and those located at 1460 and 1337 cm^{-1} to the υ_sCOO mode. The evaluation

(35) Giorgetti, E.; Margueri, G.; Sottini, S.; Casalboni, M.; Senesi, R.; Scarselli, V.; Pizzoferrato, R. J. *Non-Cryst. Solids* **1999**, *255*, 193.
(36) Carlos, L. D.; Sá Ferreira, R. A.; de Zea Bermudez, V.; Orion, I.; Rocha, J. *J. Lumin.* **2000**, *87−89*, 702.
(37) Fu, L. S.; Sá Ferreira, R. A.; Silva, N. J. O.; Carlos, L. D.; de Zea Bermudez, V.; Rocha, J. *Chem. Mater.* **2004**, *16*, 1507.
(38) Puchberger, M.; Kogler, F. R.; Jupa, M.; Gross, S.; Fric, H.; Kickelbick, G.; Schubert, U. *Eur. J. Inorg. Chem.* **2006**, 3283.
(39) Lee, J. Y.; Painter, P. C.; Coleman, M. M. *Macromolecules* **1988**, *21*, 346.
(40) Sorek, Y.; Zevin, M.; Reinsfeld, R.; Hurvits, T.; Ruschin, S. *Chem. Mater.* **1997**, *9*, 670.

Table 1. SAXS Parameters of Representative d-UZ Hybrids Obtained by Fitting Experimental Data with Eq 2

	A_1 (arb. units)	q_{Si} (Å^{-1})	σ_{Si} (Å^{-1})	A_2 (arb. units)	q_{Zr} (Å^{-1})	σ_{Zr} (Å^{-1})
d-UZ(15)	6.2×10^{-5}	0.248	0.10	2.0×10^{-4}	0.27	0.28
d-UZ(40)	3.9×10^{-4}	0.294	0.19	1.1×10^{-4}	0.45	0.13
d-UZ(50)	1.5×10^{-5}	0.323	0.1	6.5×10^{-5}	0.37	0.17
d-UZ(60)	3.1×10^{-4}	0.354	0.21	2.9×10^{-4}	0.424	0.11
d-UZ(75)	1×10^{-4}	0.290	0.2	1.9×10^{-4}	0.420	0.14

of the wavenumber difference between the 1529 and 1460 cm^{-1}bands ($\Delta\bar{\nu} \approx 69$ cm^{-1}) may be interpreted as an indication that some carboxylate groups also adopt a chelate configuration to coordinate to Zr atoms.

The band discerned at 1644 cm^{-1} both in FT-IR and Raman spectra (Figure 5 and Figure S3 of the Supporting Information, respectively), associated with the stretching vibration of the C=C groups of the methacrylate moieties (υC=C)[38,41] proves that all the samples contain unsaturated vinyl groups. The wagging vibration mode of the C=CH$_2$ groups gives rise to the band discerned at 939 cm^{-1}.[41] The presence of both features suggests that the C=C bonds remain unaffected within the composition range studied, a result that is in perfect agreement with the ^{13}C CP/MAS NMR data.

The absorption characteristic of Zr−O−Si bridges, expected at ~851 cm^{-1} [42] is missing in the FT-IR spectra of Figure 5. This result may be interpreted as a clear indication that in all the xerogels homocondensation was favored over heterocondensation, confirming the conclusions retrieved from other techniques discussed above. The band observed at 663 cm^{-1} (Figure 5) is assigned to the stretching vibration mode of the Zr−O groups.[43]

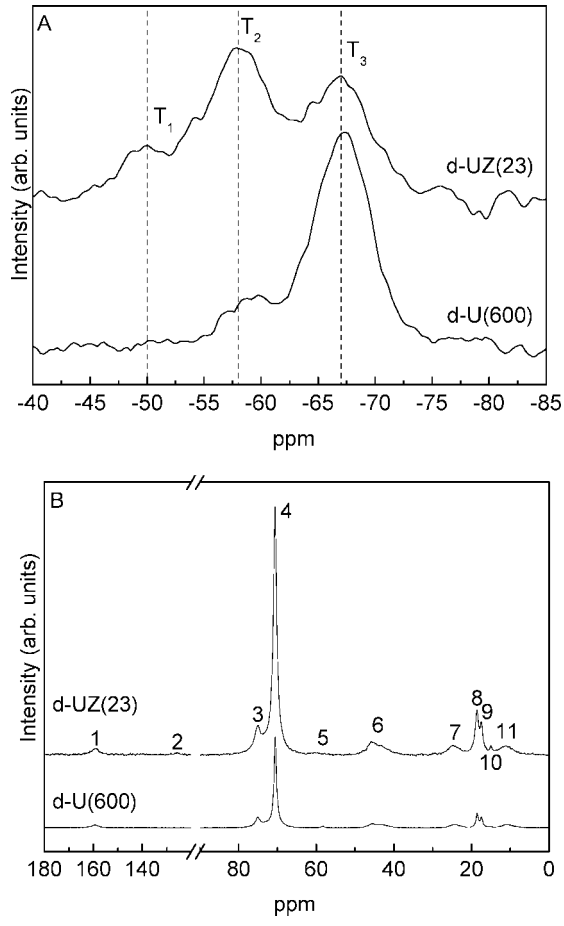

Figure 4. (A) ^{29}Si and (B) ^{13}C MAS NMR spectra of d-U(600) and d-UZ(23). (1) −N(C=O)N−, (2) CH$_2$ in McOH (Scheme 1), (3) −OCH−, (4) −(OCH$_2$CH$_2$)−, (5) −CH$_2$− in −(CH$_3$CH$_2$O)$_3$Si−, (6) −NCH$_2$− in −N(CH$_2$)$_3$Si−, (7) −CH$_2$− in −N(CH$_2$)$_3$Si−, (8) −CH$_2$− in −(OCH$_2$CH(CH$_3$))−, (9) −CH$_3$− in −(CH$_3$CH$_2$O)$_3$Si−, (10) −CH$_3$− in McOH, and (11) −CH$_2$Si− in −N(CH$_2$)$_3$Si−.

3.2. UV Patterning. Monomode waveguides were written without the need of photoinitiators through the exposure of the hybrid monoliths to UV light. The hybrids' exposed surface suffered a contraction and waveguide channels were shaped inside the monolith, underneath the exposed area. Then UV patterned diffraction gratings were superimposed to the waveguides forming Fabry−Perot cavities. Figure 6A shows a diffraction grating written in the middle of a short length waveguide previously patterned in the d-UZ(23) monolith, that presents low root-mean-square roughness values with acceptable Zr-OMc clusters homogeneity. The grating pitch Λ was estimated by fitting the data of Figure 6A to a sinusoidal function revealing a periodic refractive index perturbation with a Λ value of 525 nm (Figure 6B). The reflection spectrum (Figure 6C) was monitored and a peak (λ') around 1592 nm was found, indicating the feasibility of the use of these hybrids as band-pass optical filters, with foreseen application in optical communications. Based on the filtered wavelength and the grating pitch, the effective refractive index (n_{eff}) in the propagating region could be estimated using the following equation

$$\lambda' = 2n_{eff}\Lambda \quad (3)$$

the value being 1.5162. Although the control over the refractive index of the di-ureasil-zirconium oxo-cluster hybrids is not addressed in the present manuscript in detail,

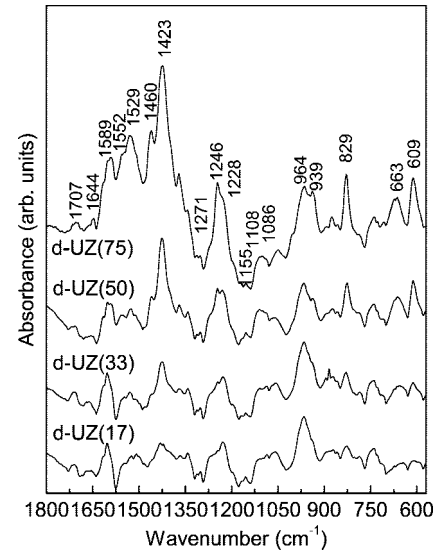

Figure 5. FT-IR spectra of the d-UZ(17), d-UZ(33), d-UZ(50), and d-UZ(75) hybrids.

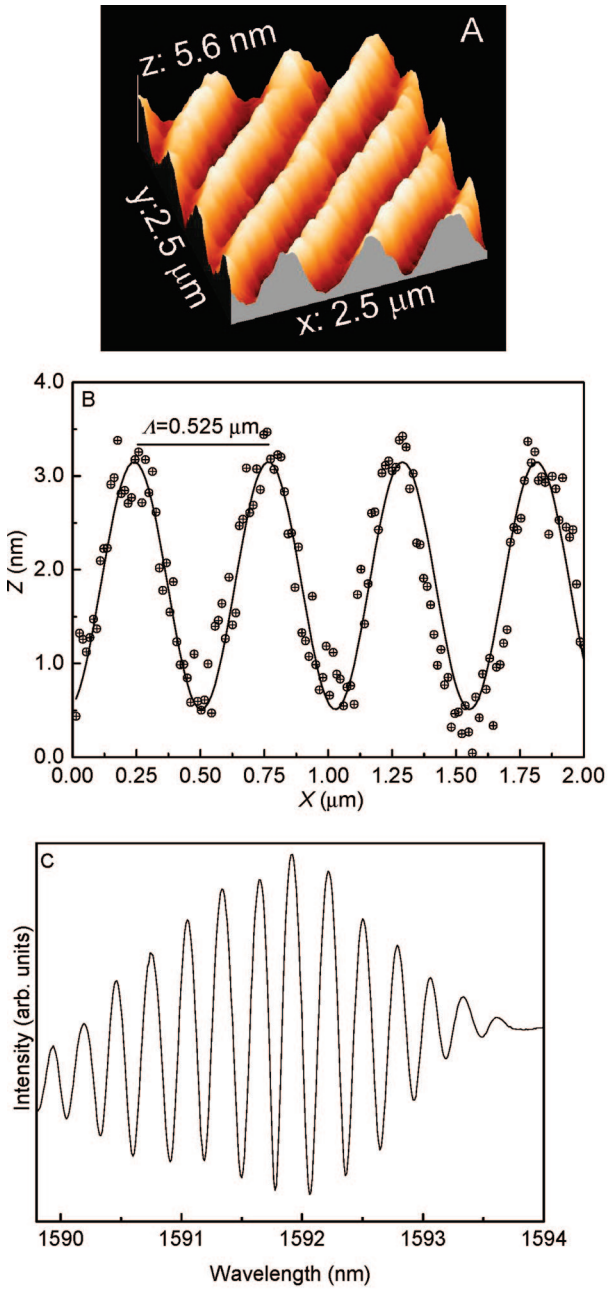

Figure 6. (A) AFM image of a diffraction grating written inside a channel in the d-UZ(23) monolithic sample with a laser rate of 0.03 mm/s. (B) Experimental (circles) and sinusoidal fitting curve (solid line) of the diffraction grating periodic structure. (C) Reflection spectrum of the diffraction grating and resonance cavity.

it can be achieved through Zr-OMc addition (the refractive index increased from 1.5040 ± 0.0005 to 1.5143 ± 0.0005 as the Si:Zr ratio increases from 1:5, d-UZ(5), to 1:45, d-UZ(31), respectively)[26] and therefore we expect larger n_{eff} values for diffraction gratings patterned in d-UZ hybrids with larger Zr-OMc amounts. These values are very close to that estimated for the effective refractive index in the propagating region (1.5162), pointing out a small refractive index contrast induced by the UV exposure, with a maximum index contrast on the order of 1×10^{-4}.

The reflection coeficient of the Fabry−Perot cavity, given by eq 1, is 0.042. This value is similar to those observed in cavities formed by two gratings.[44] The observed grating

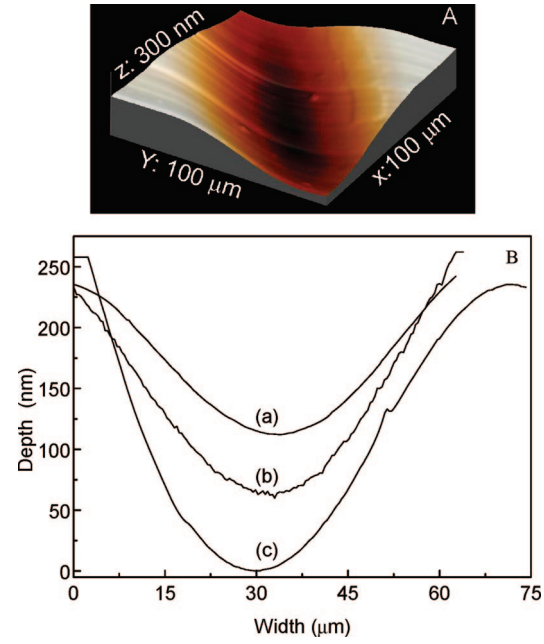

Figure 7. (A) AFM image in 3D view of the d-UZ(33) monolith surface exposed to UV. (B) Cross-section profile channels produced at different laser rates exposition (a) 0.06, (b) 0.04, and (c) 0.02 mm/s obtained from AFM measurements in the d-UZ(33) hybrid.

reflection spectrum is convolved with the transfer function of the optical resonant cavity with a free spectral range (FSR) given by

$$FSR = \frac{\lambda'^2}{2n_{\text{eff}}l} \tag{4}$$

where l is the cavity length, which in our case is 0.278 cm. From this expression, a FSR of 0.300 nm (35.5 GHz) was estimated. This value is very close to the experimental FSR value (0.286 nm), obtained from the maxima separation in the reflection spectrum (Figure 6C). This kind of structures have been used for the realization of high bit rate all optical functions, such as optical clock recovery.[45]

With the goal of further quantifying the waveguiding mechanisms, the hybrids' surface was analyzed by AFM. Figure 7A shows that the hybrids' surface exposed to UV with a laser rate of 0.02 mm/s displays a material densification with a Gaussian shape arising from the beam spectral distribution. The respective cross section profile is plotted in Figure 7B, revealing that the contraction dimension is approximately 250 nm in terms of depth with a fwhm of 35 μm. The effect of the UV exposure time on the surface densification was studied at higher laser translation rates (0.02−0.06 mm/s). The hybrids surface suffered a densifi-

(41) Colthup, N. B.; Daly, L. H.; Wiberley, S. E. *Introduction to Infrared and Raman Spectroscopy*; Academic Press: New York, 1990.
(42) Jansen, M.; Guenther, E. *Chem. Mater.* **1995**, *7*, 2110.
(43) Laaliz, I.; Larbot, A.; Julbe, A.; Guizard, C.; Cot, L. J. *Solid State Chem.* **1992**, *98*, 393.
(44) Yang, X.; Chunliu, Z.; Ng, J.; Zhang, J.; Dong, X.; Ng, K.; Guo, X.; Zhou, X.; Lu, C. *J. Opt. Commun.* **2004**, *231*, 227.
(45) Beleffi, G.; Curti, F.; Forin, D. M.; Guglielmucci, M.; Teixeira, A.; Nogueira, R.; Andre, P.; Fiorelli, A.; Reale, A.; Betti, S. In *Proceedings of Lasers and Electro-Optics Conference*, Baltimore, MD, May 22−27, 2005; Institute of Electrical and Electronics Engineers: Piscataway, NJ, 2005.

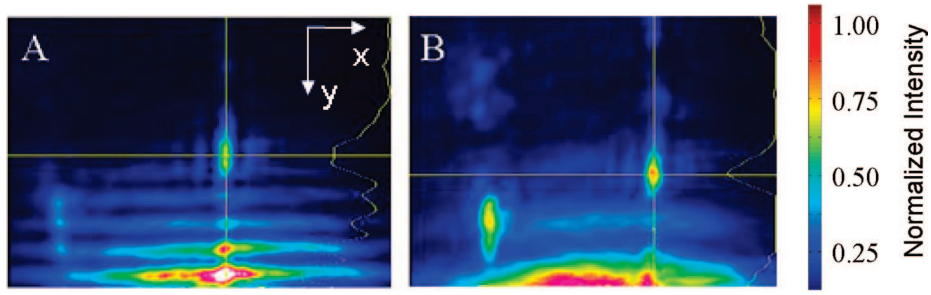

Figure 8. Mode field distribution excited at 632.8 nm in the waveguide area (A) center ($x = 0$, $y = 40$ μm from the patterned hybrid surface) and (B) $x = 36$, $y = 40$ μm. The waveguide surface Loyd interference is visible at the bottom. In the right side of each image, the intensity histogram along the vertical yellow line is displayed.

cation, whose contraction dimensions depended on the exposure time, in such a way that upon increasing the exposition time, a deeper and wider densification region resulted (Figure 7B). The hybrids' surface contraction should result from the local UV-induced polymerization of the hybrids' surface, as it was reported for poly(methyl methacrylate).[46,47] This conclusion is supported by FT-Raman spectroscopy and XRD (Figures S3 and S4 of the Supporting Information, respectively). After UV exposure the FT-Raman spectra shows a decrease of the intensity of the band at 1644 cm^{-1}, ascribed to the stretching vibration of the C═C groups of the methacrylate moieties, as exemplified for the d-UZ(33) (Figure S3 of the Supporting Information), confirming the UV photopolymerization of the methacrylate groups of the Zr-OMc NBBs. The main changes in the XRD patterns after UV exposure are found in the low-angle region, as exemplified in Figure S4 of Supporting Information. The peak at $2\theta = 3.8°$ (associated to the correlation distance between siliceous domains, Figure 1) shifts to lower angles, indicating an increase in the d_{Si} distance due to the C═C polymerization occurring in the Zr-based clusters. Because of the hybrids' surface polymerization, the Zr-OMc aggregates (Figure S1 of the Supporting Information) are dragged toward the interior of the waveguide region due to the hybrids' surface densification, which are responsible for a refractive index increase in the region underneath the exposed area, where the waveguide region was formed. A comparison between the AFM images of the UV exposed and unexposed hybrids' surface unequivocally demonstrates the absence of the Zr-OMc aggregates in the hybrids' surface after UV exposure (Figures S1, S5, and S6 of the Supporting Information).

To get further insight into the mechanisms behind the light propagation in these materials, the characterization of the effective propagating region dimensions and number of guided modes was compulsory. The mode field distribution was acquired in the visible (632 nm) and infrared (980 nm) spectral regions using a UV exposed d-UZ(23) monolith hybrid. The light was coupled into the waveguide region and the position of the injected signal was varied along the width and height of the propagating region whose frontiers were set when the output light tended to zero. From this experiment, the guidance section was determined as a Gaussian region placed below the UV-exposed surface region (Figure 7A) with typical dimensions of a 320 μm width and 88 μm depth. Figure 8A shows the mode field distribution at the center of the waveguide region displaying monomode type propagation. Moving away from the center toward the lateral limits of the guidance area allowed us to detect two propagation modes indicating a refractive index gradient within this region (Figure 8B).

Conclusions

Homogeneous transparent organic−inorganic hybrids were obtained in a system composed of methacrylate modified Zr-based oxo-clusters and poly(oxyethylene)/siloxane hybrids (di-ureasils). The structural features of these hybrids were discussed based on XRD, SAXS, AFM, FT-IR, FT-Raman, and ^{29}Si and ^{13}C NMR results. From XRD and SAXS Si- and Zr- based nanobuilding structural units were identified. The Zr-based clusters were also found in a model compound obtained from the hydrolysis of OMc-modified $Zr(OPr^n)_4$ (molar ratio 1:1). Correlation distances between these units depend on their relative concentration. NMR results showed that the condensation degree of the siloxane species were found to be lower than that observed in d-U(600) samples. The absence of Zr−O−Si heterocondensation and different coordination modes for the methacrylate groups were the main results obtained by FT-IR measurements.

These observations support a structural model where for low Zr-OMc content the Si- and Zr-based networks are interconstrained, because the Zr-based clusters are embedded in the polymeric phase between the siliceous domains, whereas segregation of the individual components at the 0.1 μm scale occurs for high contents. AFM pictures revealed the increasing size of such aggregates as the Zr-OMc relative content in the hybrids increases (∼300−500 nm). These aggregates are related to the Zr-rich phase observed in SAXS and XRD patterns.

The di-ureasil-zirconium oxo-cluster hybrids were used for the fabrication of channel monomode waveguides, diffraction gratings, and Fabry−Perot cavities obtained by UV writing without the need of photoinitiators. FT-Raman spectroscopy showed that the photochemical process that takes place under illumination is the photopolymerization of the methacrylate groups of the McOH stabilized modified

(46) Moore, J. A.; Choi, J. O. *Radiation Effects on Polymers*; Clough, R. L. Ed.; ACS Symposium Series; American Chemical Society: Washington, D.C., 1991; Vol. 475.
(47) Gupta, A.; Liang, R.; Tsay, R.; Moacanin, F. D. *Macromolecules* **1980**, *13*, 1696.

Zr-based oxo-cluster. XRD diffraction results obtained before and after patterning showed changes in the characteristic distances that were rationalized taking into account the photopolymerization process.

The guidance region was determined as a Gaussian section located below the patterned channel with typical dimensions of 320 μm wide and 88 μm deep. The effective refractive index (1.5162) and the maximum index contrast ($\sim 1 \times 10^{-4}$) were determined and a resonant cavity was formed by a grating patterned on a short length channel (0.278 cm). The reflection coeficient of the Fabry−Perot cavity reflectors was 0.042 with a FSR value of 35.6 GHz which makes it adequate to be used in optical clock recovery in optical signals with bit rate of 35.6 Gbit/s. These features demonstrate the feasibility of the use of di-ureasils containing McOH-modified $Zr(OPr^n)_4$ as low-cost components in PONs operating at high bit rate optical signals, opening up, therefore a new window of applications for these multifunctional hybrid materials.

Acknowledgment. The support of NoE "Functionalised Advanced Materials Engineering of Hybrids and Ceramics" (FAME) is gratefully acknowledged. This work was also supported by Fundação para a Ciência e Tecnologia (Portuguese agency), FEDER and POCI programs under Contract POCI/CTM/59075/2004, FAPESP and CNPq (Brazilian agencies), and CAPES-GRICES Brazil−Portugal cooperation program, Contract BEX 2866/05−6. The authors thank the help of LNLS staff and Lauro Maia (UNESP) during the SAXS and mode field distribution measurements, respectively. N.J.O.S. and A.G.M. acknowledge grants from FCT (SFRH/BD/10383/2002 and SFRH/BD/28433/2006, respectively).

Note Added after ASAP Publication. In the version of this paper published to the Web on May 10, 2008, the wrong graphic appeared for Figure 1. The paper was republished with the correct figure on May 17, 2008.

Supporting Information Available: Figures S1−S6 (PDF). This material is available free of charge via the Internet at http://pubs.acs.org.

CM7031702